

Oxidation of cyclohexane with molecular oxygen in presence of characterized macrocyclic heteronuclear FeCu complex catalyst ionically bonded to zirconium pillared montmorillonite clay

K.S. Anisia, A. Kumar*

Department of Chemical Engineering, Indian Institute of Technology Kanpur, Kanpur 208016, India

Received 18 January 2007; received in revised form 23 February 2007; accepted 26 February 2007

Available online 1 March 2007

Abstract

Heteronuclear macrocyclic complex of iron and copper, $\text{FeCuL}(\text{NO}_3)_2 \cdot 4\text{H}_2\text{O}$ [$\text{L} = (\text{CH}_3\text{C}_6\text{H}_2\text{CH}_2\text{O}(\text{CH}_2)_3\text{N})_2$] was synthesized and characterized using CHN and X-ray crystallography. A general scheme for bonding the complexes ionically on acidified montmorillonite clay was evolved and the thermogravimetric analysis of the final catalyst showed that it was stable up to 400 °C. The increased thermal and chemical stability of the complex bonded to the clay has been explained through enhanced interactive energy between them and its higher catalytic efficiency has been demonstrated through the following reaction. The oxidation of cyclohexane in presence of this catalyst using molecular oxygen in the absence of initiators, promoters and coreactants was studied in the temperature range of 150–210 °C. All commercial catalyst reported are known to form cyclohexanol and cyclohexanone in about equimolar ratio, but with our catalyst, cyclohexanone along with small amount of uncharacterized waste products (D) were formed and the selectivity of the former decreases (due to the formation of large amount of D) with increase in temperature. The experimental data were analyzed against different kinetic scheme available in literature and the rate constants of the best scheme were determined using Genetic Algorithm. From the experiments carried out at different temperatures and pressures, we found that for every rate constant, an Arrhenius type relation (independent of reactor pressure) could be established.

© 2007 Published by Elsevier B.V.

Keywords: Macrocyclic complex; Cyclohexane oxidation; Montmorillonite clay; Genetic algorithm; Molecular oxygen

1. Introduction

The partial oxidation of hydrocarbons using oxygen is significant to the petrochemical industry in converting petroleum hydrocarbon feedstock into important functionalized chemicals. However, in doing this, the desired partially oxidized products are further oxidized eventually converting it to CO_2 and the C–H bond energies are different for primary, secondary and tertiary (reducing in this order) positions. So in order to attain high selectivity for the target products, the conversions of the oxidation process are usually kept very low and the success of an industrial reaction depends on the stringent control of the temperature and pressure. The partial oxidation of cyclohexane to cyclohexanone and cyclohexanol is one of the industrially important process as they serve as starting materials for the production

of polymers such as Nylon-6 and Nylon-6,6. Cyclohexanone is used in the production of caprolactam which is utilized in the manufacture of Nylon-6 and cyclohexanol is converted to adipic acid for the manufacture of Nylon-6,6 [1]. The oxidation of cyclohexane is carried out industrially in the temperature range of 423–453 K and pressure of 1.0–1.6 MPa in presence of cobalt salts (naphthenate, stearate or oleate) as catalyst. The cyclohexane conversion is kept low (about 3–4% per pass) as the cyclohexanol and cyclohexanone formed are more susceptible for further oxidation to CO_2 . At the industrial condition, the products such as adipic, succinic and oxalic acids and their cyclohexyl esters (designated as one single product D in all catalytic studies reported in literature) are always formed which need to be separated first [1,2]. The alternate route to cyclohexanol and cyclohexanone involves hydrogenation of phenol, a reaction that gives a selectivity of more than 97% at 99% conversion but the process economics favors direct oxidation of cyclohexane [3]. Catalytic oxidation studies in the literature have been conducted using oxidants (other than molecular oxygen)

* Corresponding author. Tel.: +91 512 259 7195; fax: +91 512 259 0104.
E-mail address: anilk@iitk.ac.in (A. Kumar).

such as hydrogen peroxide, *t*-butyl hydrogen peroxide (TBHP) but molecular oxygen is the cheapest [4].

To overcome the problem of separating the catalyst from the reaction mass, many heterogeneous catalysts have been developed for this reaction. Generally these catalysts are either oxides or metal cations incorporated in inorganic matrices such as silica, alumina, zirconia, active carbon, zeolites [5] or aluminophosphates [6]. The activity of these systems also depends on the correct choice of the solvent, which determines the polarity of the medium and the active catalytic metal adsorbed on the surface of the support. For example, during the oxidation of cyclohexane in presence of CoAPO-5 catalyst, the use of carboxylic acids (except formic acid) as the solvent is necessary and the use of propionic acid gives the highest reaction rate [7]. The other problems encountered in heterogeneous catalysis is leaching of active metal ions, extreme reaction conditions (2 MPa pressure and 177 °C temperature) and low activity [8]. An induction time is generally observed in the case of air oxidation of cyclohexane and is reduced by adding promoters or co-reactants such as acetaldehyde, cyclohexanone, cyclohexanol and azobiz(isobutyronitrile) (AIBN) [9]. Coreactants also help in increasing the rate of cyclohexane oxidation (by decreasing the overall activation energy) and selectivity (ratio of desired product cyclohexanone and the total product formed) of the target products and minimizing the formation of D. Experiments have shown that water formed during the reaction has a retarding effect due to phase separation [10].

The mechanism suggested in the literature assumes that cyclohexyl hydroperoxide (CHHP) is the intermediate formed in the presence of transition metal salts and sometimes a small quantity of this has been detected in the product stream [10]. The main products of its decomposition are cyclohexanol and cyclohexanone and are usually present in the product stream approximately in equimolar ratio. The primary effect of dissolved metal salts on the oxidation reaction is to increase the rate of reaction by catalyzing the homolytic decomposition of hydroperoxides [11].

The mechanism of cyclohexane oxidation proposed in literature is a multistage, free radical chain reaction, comprising of initiation, chain propagation and chain termination step. Tolman et al. [12,13] developed a reaction scheme consisting of 154 reactions which is impractical to analyze as it requires the determination of as many number of rate constants simultaneously with high accuracy. Hence lumped kinetic models which require lesser rate constants have been developed and the models available in literature [14–16] are shown in Fig. 1 and are discussed below. In the first model, cyclohexane forms a hydroperoxide which is then converted into cyclohexanone, cyclohexanol and unidentified waste products (D). In the second model, the formation of hydroperoxide is not considered, but further oxidation of cyclohexanol is terminated by the reaction with boric acid forming boric esters. An exhaustive model for non catalytic oxidation which consisted of 19 reactions and 10 species has been given in the literature [16]. They estimated the rate constants and the concentration of the intermediate free radicals RO_2^* , RO^* , R^* and OH^* in solution. Pohorecki et al. [17] suggested a lumped kinetic model for the catalytic oxidation

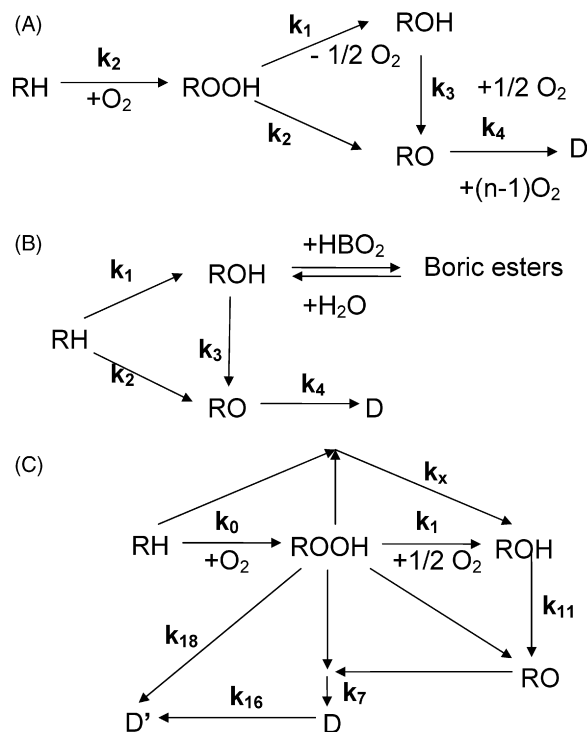
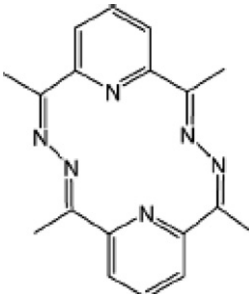
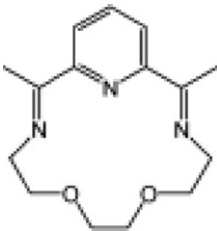
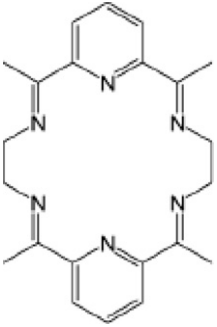
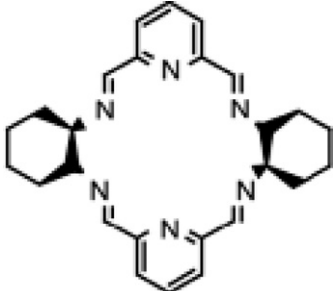


Fig. 1. Kinetic models available in literature for oxidation of cyclohexane.

of cyclohexane. The reaction scheme consisted of 7 reactions and the quasi steady state hypothesis was applied for estimating the free radical species RO_2^* , RO^* and R^* in the solution. The reactive byproducts in the liquid phase and the non-reactive byproducts in the gas phase were also incorporated in their model. The catalyst was thought to influence the initiation and the propagation steps and principal pathways were considered for global kinetics of the oxidation reaction. The role of the catalyst was introduced into the model by assuming specific forms of dependency of reaction rate constants on the catalyst concentrations.

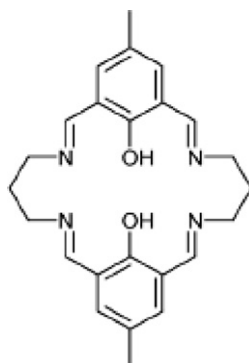
Study of literature indicates the use of multimetallic catalyst to improve the catalytic efficiency and selectivity and the work reported in this study is an effort in this direction. We observed that using multimetallic catalyst, the heat of mixing ΔH_m , for different salts determines the state of the metal on the support (as ideal solution, solid solution, ordered solution, mono or biphasic solution or surface alloys) and this way affecting the performance of the catalyst [18]. The use of multimetallic complexes is a step towards developing a system which is independent of ΔH_m . Even though complexes have been known in the early development of modern chemistry, their application in catalysis has been limited due to low thermal stability and literature has mainly focused on their preparation and properties. As catalyst, these complexes are expected to provide new reactivity patterns because the interaction between the metals and the ligand would help in promoting reaction due to the unique charge distribution around it. Some of the complexes that have been used in catalytic chemical reactions are given in Table 1 [19–38] where in column 5 the reactions catalyzed by these complexes are given and are seen to be mostly bio-

Table 1
Some of the macrocyclic complexes used for chemical reactions

Names	Ligands	Structure	Metals	Usage	Ref.
Tetradentate Schiff base complex	2,6-Diacetylpyridine + hydrazine		Scandium, zinc(II), magnesium(II)	Site-specific DNA oxidation	[19]
Pentadentate Schiff base complex	2,6-Diacetylpyridine + 1,8-diamine-3,6-dioxaoctane		Yttrium(III), dysprosium(III), erbium(III), thulium(III), lutetium(III)	Biological systems	[20]
Hexadentate Schiff base complex	2,6-Diacetylpyridine + ethylenediamine (or 0-phenylenediamine)		Lanthanum(III), cerium(III), praseodymium(III) and neodymium(III)	Synthetic nucleases catalysts for RNA transesterification	[21]
Chiral Schiff base macrocycles	2,6-Diformylpyridine + R,R- or S,S-1,2-diaminocyclohexane		lanthanide(III)	Artificial catalysts for hydrolytic DNA cleavage	[22]

Hexadentate macrocycles derived from 2,6-diformylphenols (Robson ligand)

2,6-Diformylphenol + 1,3-propylenediamine



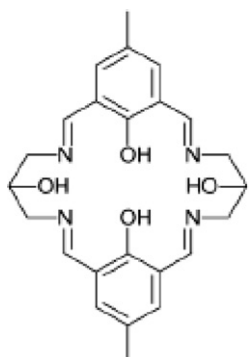
Cu(II), Cu(I), Ni(II), Zn(II), Fe(II), Fe(III), Pd(II) and Ru(III)

Metalloenzymes

[23]

Hexadentate macrocycles derived from 2,6-diformylphenols (Robson ligand)

2,6-Diformyl-4-methylphenol + 1,3-diamino-2-hydroxypropane



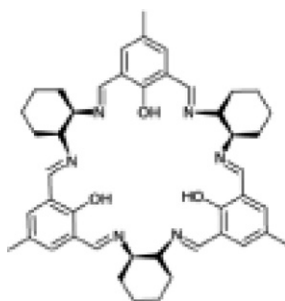
La(III), Ce(III) and Eu(III) ions

Biomedical applications

[24]

Hexadentate macrocycles derived from 2,6-diformylphenols (Robson ligand)

2,6-Diformylpyridine + 1,2-diaminocyclohexane



Zinc(II)

Biomedical applications

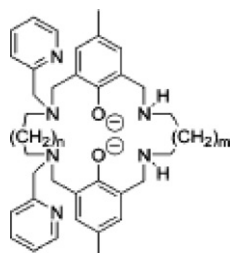
[25]

Table 1 (Continued)

Names	Ligands	Structure	Metals	Usage	Ref.
Macrocyclic complexes of tetraaminodiphenols	2,6-Diformyl-4-R-phenol (R = H, Me, F) + 4,4''-diamino-3,3'',5,5''-R' ₄ -o-terphenyl (R' = iPr, Et)		Nickel	Ethylene polymerization	[26]
Macrobicyclic complexes	5-Methylsalicylaldehyde + 3,4:10,11-dibenzo-1,13[N,N'-bis{(3-formyl-2-hydroxy-5-methyl)benzyl}diaz]-5,9-dioxocycloheptadecane		Nickel(II)	Hydrolysis of 4-nitrophenylphosphate	[27]
Heteronuclear bimetallic macrocyclic complexes	2,6-bis(Iminomethyl)-4-methylphenolate + $-(CH_2)_mNH(CH_2)_m-$ ($m = 2, 3$)		Cu, Mn, Cu, Fe, Cu, Co, Cu, Pb, Di Cu	Supramolecular chemistry	[28]

Homonuclear bimetallic
macrocyclic complexes

Dialdehyde + diamine



$n = 0, 1; m = 0, 1$

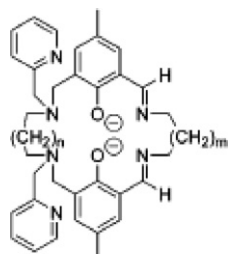
DiCo, DiZn, DiFe

Bimetallic reactivity

[29]

Heteronuclear bimetallic
Macrocyclic complexes

Dialdehyde + diamine



$n = 0, 1; m = 0, 1$

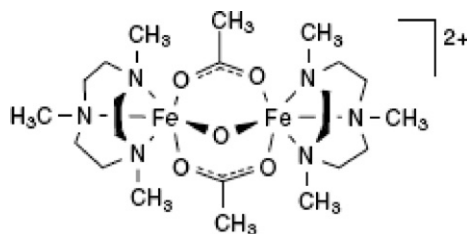
DiCo, DiNi, DiMn, Cu-Zn,
Co-Mn

Bimetallic reactivity

[30]

Triazacyclononane
ligands

Cyclononane + triethylamine

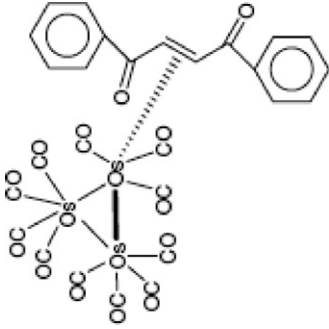
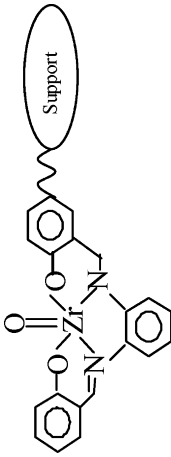


DiCo, DiFe, DiMn

Bimetallic reactivity

[31,32]

Table 1 (Continued)

Names	Ligands	Structure	Metals	Usage	Ref.
(2,3- <i>g</i> -1,4-Diphenylbut-2-en-1,4-dione)undecacarbonyltriangulotriosmium	–		Os	Bimetallic reactivity	[33]
Salen complexes supported on alumina and Silica	[1,4- <i>bis</i> (Salicylidene amino)-phenylene]		Zr, Co, V	Catalyst	[34–38]

logical in nature for which temperatures required are close to room temperature. Use of complexes for catalysis beyond 50 °C is not known because of their thermal and chemical instabilities in harsh environments and has never been used for industrial reactions.

In our present work, we have synthesized a heteronuclear macrocyclic iron copper complex, $\text{FeCuL}(\text{NO}_3)_2 \cdot 4\text{H}_2\text{O}$ [$\text{L} = (\text{CH}_3\text{C}_6\text{H}_2\text{CH}_2\text{O}(\text{CH}_2)_3\text{N})_2$] and ionically bonded to the zirconium pillared montmorillonite clay to form the heterogeneous catalyst. We have studied the oxidation of cyclohexane with these catalysts at various temperatures in the temperature range 145–200 °C. The products formed were identified by Gas Chromatography Mass Spectroscopy (GCMS) analysis and unlike other catalysts (which form cyclohexanol and cyclohexanone in almost equimolar amount) in the case of our catalyst only cyclohexanone was formed. In this paper we show that the FeCu heteronuclear complex serves as an effective catalyst for the oxidation of cyclohexane and does not require co-catalyst, solvent, promoters and initiators. The catalysts described in literature forms cyclohexanone and cyclohexanol in equimolar ratio and in contrast to this our catalyst gives cyclohexanone in considerably large amount. Based on the literature we have proposed a ligand centered reaction mechanism in which the hydroperoxide species are adsorbed on the complex catalyst. We have then written the differential mole balance relations for all intermediate as well as the reacting species and we integrated them for specified rate constants using fourth order the Runge–Kutta technique. The guess values needed for running the simulation were randomly varied in accordance with the Genetic Algorithm (GA) and the total mean error between the experimental and simulated concentration of all species were minimized. Our study shows that for the temperature range studied, the optimal rate constants can be expressed in the usual Arrhenius form and are independent of the concentrations of the species in the reaction mass.

2. Experimental studies

2.1. Preparation of the macrocyclic complex

The brownish yellow crystals of 2,6-diformyl-4-methylphenol needed for the macrocyclic complex was prepared following the procedure given in literature [39]. The ^1H NMR spectrum of the dialdehyde prepared by us shows singlets at 11.42 ppm (phenolic proton), 10.2 ppm (aldehydic), 7.74 ppm (aromatic) and 2.36 ppm (methyl) and is consistent with that of the assigned structure and matches with that given in literature [39]. In order to prepare the macrocyclic ligand the 2,6-diformyl-4-methylphenol is condensed with 1,3-diaminopropane in two stages forming FeL' and FeCuL . This gives two identical N_2O_2 sites in the ligand.

2.2. Synthesis of $\text{FeCuL}(\text{NO}_3)_2 \cdot 4\text{H}_2\text{O}$

[$\text{L} = (\text{CH}_3\text{C}_6\text{H}_2\text{CH}_2\text{O}(\text{CH}_2)_3\text{N})_2$] macrocyclic complex

FeL' : To 50 ml of *N,N*-dimethylformamide at 40 °C, 2,6-diformyl-4-methylphenol (1.95 g, 0.012 mol) was added first,

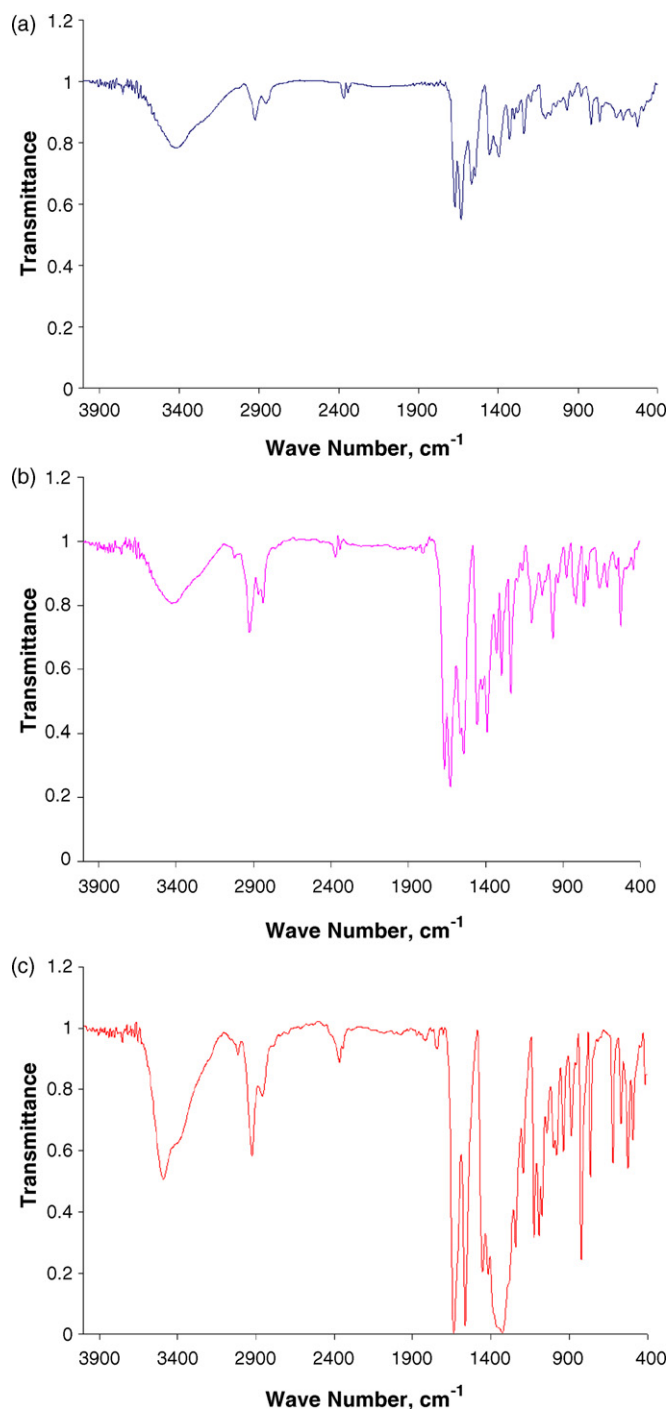


Fig. 2. (a) FTIR spectra of FeL' which is formed in step I of the complex synthesis. (b) FTIR spectra of $FeCuL'$ which is formed in step II of the complex synthesis. (c) FTIR spectra of $FeCuL$ complex which is formed in step III.

followed by drop wise addition of (0.5 ml, 0.006 mol) of 1,3-diaminopropane with stirring. To this solution (2.5 g, 0.006 mol) of ferric nitrate was added and the solution was stirred till all the ferric nitrate had dissolved completely. The solution was kept for 1 h after which diethyl ether was added, which a precipitate appeared which was filtered and dried. The FTIR spectrum (Fig. 2a) shows the presence of functional groups C=N at 1541 cm^{-1} and C=O at 1671 cm^{-1} .

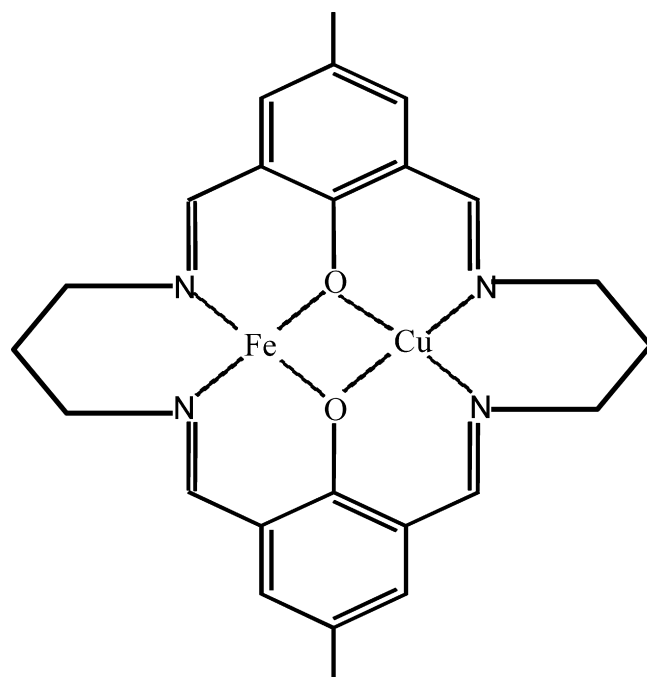


Fig. 3. Structure of the $FeCu$ macrocyclic complex based on the data of Tables 1 and 2.

$FeCuL'$: The FeL' (1.9 g, 0.0045 mol) obtained from the previous step was dissolved in 30 ml of methanol and to this (0.9 g, 0.0045 mol) of cupric acetate dissolved in methanol was added with stirring. After 1 h, diethyl ether was added and within 30 min olive green precipitate was formed which was filtered and dried. The FTIR spectrum (Fig. 2b) shows the presence of functional groups C=N at 1540 cm^{-1} and C=O at 1666 cm^{-1} .

$FeCuL$: The $FeCuL'$ (1.83 g, 0.0038 mol) was dissolved in 30 ml of methanol and to this, a solution of 1,3-diaminopropane (0.3 ml) was added drop wise with stirring. The solution was kept for 30 min and then diethyl ether was added to it. A precipitate was formed which was filtered from the solution and dried. The FTIR spectrum (Fig. 2c) of the complex shows C=N at 1532 and the C=O peak does not appear as it forms C=N bond on reaction with 1,3-diaminopropane. The structure of the final complex is given in Fig. 3. To confirm the formation of the complex, the 1H NMR spectrum of the complex dissolved in d_6 -DMSO was taken and it shows singlets at 9.149 (phenolic), 3.378 and 2.072 ppm (aliphatic). The higher intensity at 2.072 ppm shows that the methyl peaks are overlapping with the aliphatic protons of the diaminopropane.

2.3. Preparation of the heterogeneous catalyst

The acid (using HCl) treated montmorillonite was procured from Ashapura Minechem Ltd., Mumbai, India and was first pillared using zirconium ions and then was intercalated with the complex as shown in Fig. 4. The clay (20 g) is subjected to swelling by adding water (1 l) to the clay and stirring it for 5 h and the mixture was finally centrifuged and dried. In the next step, the clay was treated with NaCl solution (1 M) and this was aged for 24 h. The clay was separated, dried and then refluxed

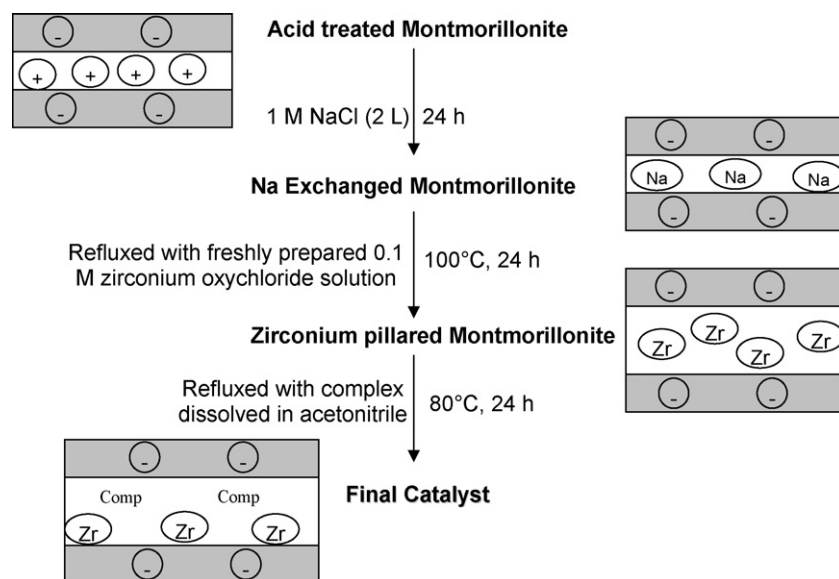


Fig. 4. General scheme for catalyst preparation. Total amount of complex on the final catalyst is 0.9 g.

with freshly prepared zirconium oxychloride (0.1 M) solution for 24 h at 100 °C to obtain zirconium pillared montmorillonite. The final step is the intercalation of the complex in the clay layers and is shown in this figure. The clay from the previous step was taken and refluxed with the complex dissolved in acetonitrile for 24 h at 80 °C and the final catalyst thus obtained was separated, washed with acetone and dried.

2.4. Reaction procedure

The oxidation reactions were performed in a high-pressure stainless steel reactor. An autoclave-rocking reactor having capacity of 300 ml with gas delivery system, and sampling line was employed for the reaction. The reactor was initially charged with 100 ml cyclohexane and 1 g of catalyst, heated to the required temperature for the desired reaction time using oxygen as the oxidant. An on/off controller was used for controlling the temperature with a chrome alloy thermocouple for temperature sensing. The products obtained after reaction were analyzed by gas chromatography (GC) using a fused silica capillary column 0.25 mm × 50 m film thickness 0.25 μm with flame ionization detector and the gas chromatography mass spectroscopy (GC–MS) was carried out using a Shimadzu QP-2000 instrument.

2.5. Test for the absence of cyclohexyl hydroperoxide in the reaction mass

The presence of cyclohexyl hydroperoxide in the product mixture can be detected by adding excess triphenylphosphine to the product formed. The increase in the intensity of the peak corresponding to the alcohol in the GC analysis of the reduced sample confirmed the presence of cyclohexyl hydroperoxide molecule [40,41]. In the presence of our catalyst, we have shown that on carrying similar experiments by adding triphenylphosphine, the peak intensity of the cyclohexanol in the GC analysis of

the original product and the reduced sample remains unchanged. Thus, it was concluded that there cyclohexyl hydroperoxide was not detected in the product mixture.

3. Results and discussion

3.1. Catalyst characterization

3.1.1. FTIR analysis of the complex

The FTIR analysis was carried out on a Bruker Vector 22 instrument in the 4000–400 cm⁻¹ wave number range. The samples were ground with KBr and pressed to 1 mm thick film. Examination of the FTIR spectra (shown in Fig. 2a–c) were useful in confirming that the formation of the complex and its various intermediates. This is determined based on the frequencies of the C=N (1541 cm⁻¹ in step I, 1540 cm⁻¹ in step II and 1532 cm⁻¹ in step III) and C=O bond. The C=O bond frequency (1671 cm⁻¹ in step I and 1666 cm⁻¹ in step II) disappears in the final step (as seen in Fig. 4c) when the complex *FeCuL'* is reacted with 1,3-diaminopropane.

3.1.2. CHN analysis of the *FeCuL(NO₃)₂·4H₂O* complex

The CHN analysis was carried out in an elemental analyzer (CE 440 Leimann Labs Inc.). Helium was used as the carrier gas and 3–5 mg of the sample was required. The percentage of carbon, hydrogen and nitrogen present in the complexes were determined. The experimentally obtained values are 39.9% carbon, 3.995% hydrogen and 11.93% nitrogen. Since the complex was prepared using ferric nitrate the complex was assumed to have NO₃ ligand and its structure was assumed to be *FeCuL(NO₃)₂·4H₂O* [L = CH₃C₆H₂CH₂O(CH₂)₃N₂]. Fig. 4 gives the structure of the complex which contains 24 C, 32 H, 6 N, 12 O, 1 Fe and 1 Cu and the theoretical values of C, H and N were calculated as 40.25, 4.47 and 11.7%, respectively.

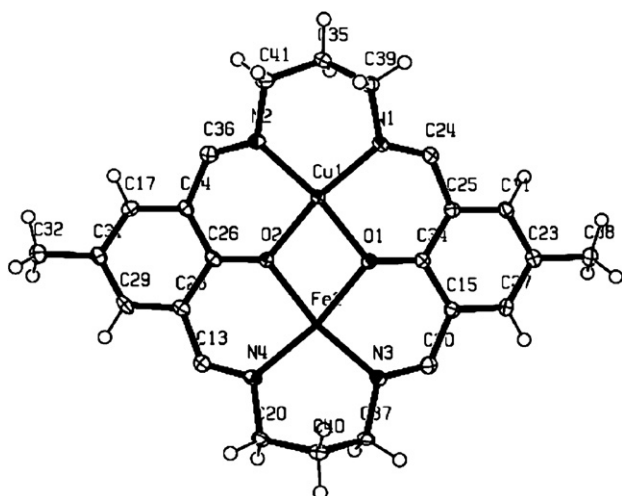


Fig. 5. Molecular structure of the FeCu macrocyclic complex as determined by single crystal X-ray crystallography.

3.1.3. Single crystal X-ray diffraction analysis of the complex

A single crystal of the FeCu macrocyclic complex was grown to study its structure by X-ray diffraction analysis. In order to grow the single crystal, the evaporation technique was used with methanol as the solvent. Diffracted intensities were collected on a Bruker SMART APEX CCD diffractometer, with graphite-monochromated Mo K α ($k=0.71073$ Å) radiation at 100 K. For data reduction Bruker saint Plus program was used and the data were corrected for absorption. The structures were solved by SIR 92, expanded by Fourier-difference synthesis and refined with the SHEIX1-97 computer package incorporated in WinGX 1.64 crystallographic collective package [42]. The position of the hydrogen atoms was calculated assuming ideal geometries and all non-hydrogen atoms were refined with anisotropic thermal parameters by full matrix least-squares procedures on F^2 . The structure of the complex obtained from the crystallographic analysis is shown Fig. 5 and the crystallographic parameters are summarized in Table 2 and the selected bond length and bond angles are given in Table 3. A SEM micrograph of the complex obtained is shown in Fig. 6.

3.1.4. Thermal stability of the complex and the final catalyst

The TGA analysis of the complex as well as the final catalyst was carried out using a Perkin-Elementer instrument in N₂ atmosphere. The FeCu complex was heated from 40 to 900 °C at the rate of 10 °C/min and it was found that the complex is stable up to 250 °C (Fig. 7). Similarly the TGA of the final catalyst was done by heating it from 40 to 700 °C at the rate of 10 °C/min and it was found that the final catalyst (indicated by large weight loss in the differential curve of Fig. 8) was stable till 400 °C (Fig. 8). This can be explained if we observe the binding of the complex in the clay as follows. As shown in Fig. 9, the montmorillonite clay comprises of a negatively charged layer composed of two tetrahedral Si–O sheet sandwiching an octahedral Al sheet with oxygen atoms at the apex shared by the octahedra with the tetrahedra. The excess negative charge is due to the partial substitution of the Al³⁺ by Mg²⁺ and in order to

Table 2
Crystal data and structure refinement parameters

Empirical formula	C ₂₄ H ₂₂ CuFeN ₆ O ₉
Formula weight	657.87
Temperature	293 (2) K
Wavelength	0.71069 Å
Crystal system, space group	Orthorhombic, <i>P</i> -1
Unit cell dimensions	$a = 8.565$ (5) Å, $\alpha = 90.000$ (5)° $b = 18.262$ (5) Å, $\beta = 90.000$ (5)° $c = 32.333$ (5) Å, $\gamma = 90.000$ (5)°
Volume	5057 (3) Å ³
Z, calculated density	8, 1.728 Mg/m ³
Absorption coefficient	1.482 mm ⁻¹
$F(0\ 0\ 0)$	2680
Crystal size	0.1 mm × 0.1 mm × 0.05 mm
Theta (θ) range for data collection	2.32–28.30°
Reflections collected/unique	32,164/6232 [$R(\text{int}) = 0.0688$]
Completeness to $\theta = 28.30$	99.0%
Absorption correction	Empirical (SADABS)
Refinement method	Full-matrix least-squares on F^2
Data/restraints/parameters	6232/0/355
Goodness-of-fit on F^2	1.053
Final R indices [$I > 2\sigma(I)$]	$R_1 = 0.0645$, $wR_2 = 0.1518$
R indices (all data)	$R_1 = 0.0794$, $wR_2 = 0.1597$
Largest diff. peak and hole	1.737 and -1.235 e Å ⁻³

achieve electroneutrality, the layer charge is compensated by the presence of cations such as Na⁺ and Ca²⁺ in the interlayers [43,44]. These are held together by weak dipolar and van der Waal forces and the distance between them is known as basal spacing or *c*-spacing [44]. In Fig. 8 we have shown the complex within the clay and the interacting force between them is equivalent to an ionic bond. There has been a considerable interest in the literature to predict the state of adsorbate in porous material and determine the phase equilibria of these [45]. In order to model these, it is assumed that the liquid is in a cage formed by the porous substances and the state of the adsorbate depended upon the pore geometry, the level of interaction between the liq-

Table 3
Selected bond lengths [Å] and angles [°]

Cu(1)–N(1)	1.956 (4)
Cu(1)–O(1)	1.960 (3)
Cu(1)–O(2)	1.961 (3)
Cu(1)–N(2)	1.980 (4)
Fe(2)–N(3)	1.949 (4)
Fe(2)–O(1)	1.967 (3)
Fe(2)–O(2)	1.970 (3)
Fe(2)–N(4)	1.981 (4)
N(1)–Cu(1)–O(1)	92.11 (14)
N(1)–Cu(1)–O(2)	169.78 (14)
O(1)–Cu(1)–O(2)	77.67 (13)
N(1)–Cu(1)–N(2)	97.73 (15)
O(1)–Cu(1)–N(2)	169.30 (14)
O(2)–Cu(1)–N(2)	92.47 (14)
N(3)–Fe(2)–O(1)	91.74 (14)
N(3)–Fe(2)–O(2)	168.41 (14)
O(1)–Fe(2)–O(2)	77.30 (12)
N(3)–Fe(2)–N(4)	99.38 (15)
O(1)–Fe(2)–N(4)	166.90 (14)
O(2)–Fe(2)–N(4)	91.96 (14)

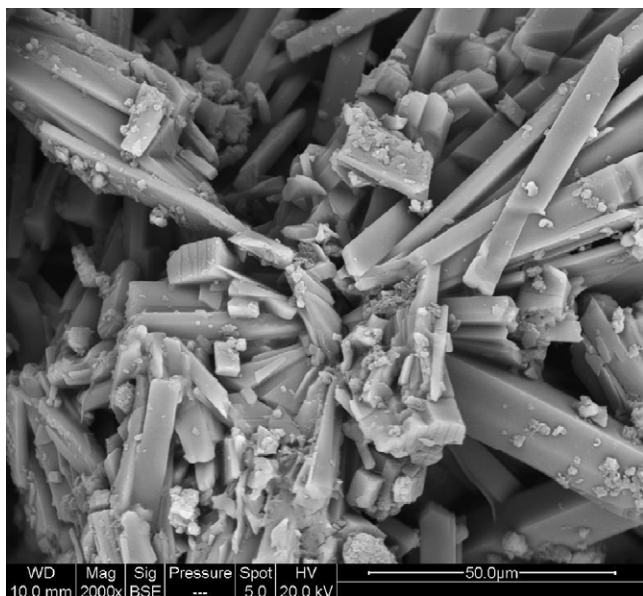


Fig. 6. SEM micrograph of the FeCu complex at 5000 magnification.

uid and pores and the chemical and geometrical heterogeneity. The observed chemical and thermal stability of the complex ionically bonded in the final catalyst may well be attributed to the cage (of Fig. 9) effect produced by the clay layers.

3.1.5. Small angle X-ray diffraction analysis

Small angle X-ray diffraction measurements were done on ARL X'TRA X-ray diffractometer (Thermo Electron Corporation) equipped with Cu K α ($\lambda = 0.154$ nm) radiation. The voltage and current applied to the X-ray tube were 45 kV and 20 mA, respectively, and the sampling width was set at 0.05° with scanning speed as 1° min^{-1} ($2\theta = 2-10^\circ$). The X-ray diffraction patterns of the original montmorillonite clay, zirconium pillared montmorillonite and final catalyst (FeCu macrocyclic complex ionically bonded to montmorillonite) is given in Fig. 10. The zirconium pillared montmorillonite was obtained by refluxing

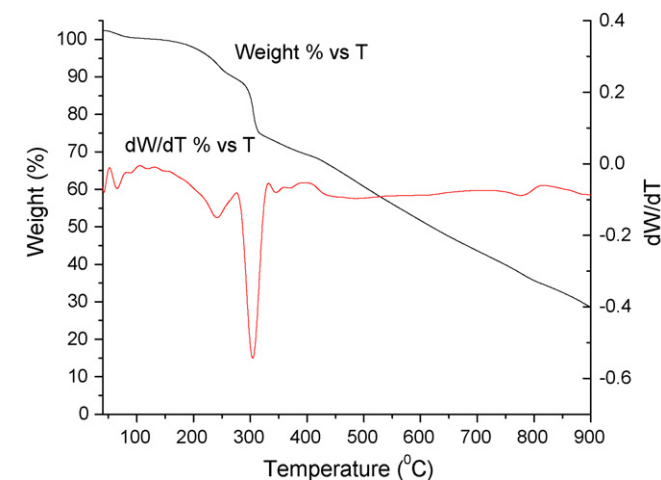


Fig. 7. Thermo gravimetric analysis of FeCu Complex. The complex is stable up to 250°C as indicated by relatively large weight loss (or dip in dW/dT) in this figure.

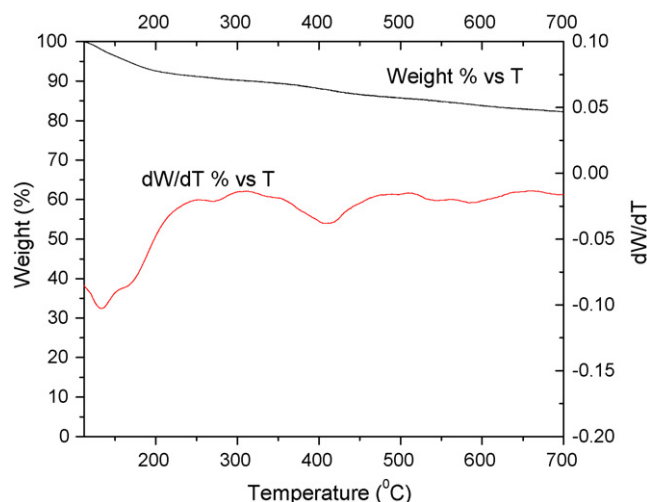


Fig. 8. Thermo gravimetric analysis of the FeCu macrocyclic complex catalyst. The catalyst is stable up to 400°C and repeated reactions using the same catalyst the conversions do not change.

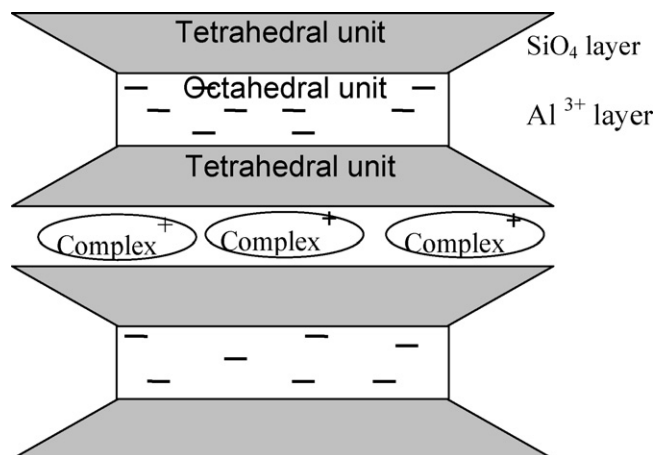


Fig. 9. The montmorillonite above has been representing by three layered structure in which the octahedral sheet is negatively charged which holds the complex macrocyclic complex by electrostatic forces.

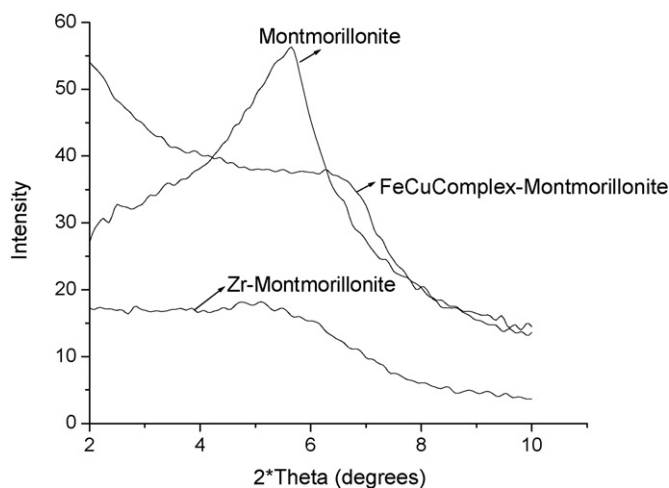


Fig. 10. Small angle X-ray diffraction pattern of the original montmorillonite clay, Zr pillared montmorillonite and final catalyst.

the Na-montmorillonite with 0.1 M freshly prepared zirconium oxychloride solution at 100 °C for 24 h. The clay was separated and dried and its weight increased by 8 g. The final catalyst was prepared by taking 20 g of zirconium pillared clay and refluxing with the FeCu complex solution (1 g of complex in 250 ml acetonitrile) at 80 °C for 24 h. The weight increased by 0.9 g after the incorporation of the complex. The *d*-spacing is calculated from the 2θ value of the peak corresponding to (001) plane and in the original montmorillonite a peak is observed at $2\theta = 5.66$ from which the *d*-spacing is calculated as 15.58 Å. The introduction of FeCu macrocyclic complex into montmorillonite resulted in the disappearance of (001) peak. This is likely to be due to the lack of ordering in the *c*-direction as a result of delamination [46] and the non-parallel ordering of aluminosilicates layers causes the delaminated structures of montmorillonite. The weak peak for Zr pillared montmorillonite and FeCu complex montmorillonite seems to occur at 5.03 and 6.8°, respectively. This suggests that the montmorillonite undergoes a slight expansion when treated with zirconium while by the introduction of the FeCu complex the clay *d*-spacing seems to shorten.

3.1.6. Surface area measurement

The surface areas of the samples were measured using single point BET method and nitrogen was used for adsorption. The analysis was done in a bench top COULTER SA 3100 apparatus and the surface area of the original montmorillonite clay, zirconium pillared montmorillonite clay and the final catalyst were found to be 331.2, 115.63 and 99.34 m²/g, respectively.

3.2. Analysis of cyclohexane oxidation reaction

3.2.1. Catalytic study

The oxidation of cyclohexane with molecular oxygen in presence of complex bonded to montmorillonite clay catalyst was conducted in the temperature range 150–210 °C. From the GC and GC–MS analysis it was found that only cyclohexanone was formed as the product along with the undesired product (D). The above temperature range was chosen because below 150 °C the conversion was very low while above 210 °C, though the conversion was high, a large amount of undesired products (D) was formed. Based on the feed and the product con-

centration the %conversion $[(N_{RC}/N_{RF}) \times 100]$, %selectivity $[(N_{PC}/N_{RC}) \times 100]$ and %yield $[(N_{PC}/N_{RF}) \times 100]$ are calculated. In these, N_{RC} is the number of moles of cyclohexane consumed, N_{RF} is the number of moles cyclohexane fed and N_{PC} is the number of moles of cyclohexanone formed. In these, the overall conversion increases from 5.7 to 12.8% when the temperature was increased from 150 to 210 °C (160 min reaction time) and a conversion of 14.4% was obtained when the reaction was conducted for at 210 °C 260 min. At 150 °C the cyclohexanone was formed with high selectivity of 95.6% and with increase in temperature, its selectivity decreases to 83.7% due to the formation of undesired side products.

3.2.2. Metal leaching test

To confirm that the metal complex is not leaching at the reaction conditions studied, we carried out the following experiments.

- I. The oxidation reactions were carried out using the spent catalyst and the conversion was found to remain unaltered. The comparison of overall cyclohexane conversion and cyclohexanone yield obtained when the reaction was carried out with fresh catalyst and spent catalyst (after 60 h of usage) at 190 and 210 °C are presented in Table 4.
- II. From the product, the catalyst was filtered and the product mixture was once again subjected to the same temperature and pressure. The overall conversion was measured before and after the catalyst was filtered and found to be unchanged indicating that there is no leaching of the active species. For example the reactor was charged with 100 ml cyclohexane, 1 g of the catalyst and pressurized with 200 psig oxygen. The reaction was carried out for 2 h at 210 °C; the overall cyclohexane conversion and cyclohexanone yield were found to be 13.8 and 11.4%, respectively. The catalyst was filtered out from this product mixture, then it was subjected to the same conditions and the reaction was carried for another 2 h, but there was no further increase in conversion.

3.2.3. Reaction mechanism

Some of the reaction mechanisms that have been found in literature are discussed. Modén et al. [47] have investigated

Table 4
Comparison of overall conversion and cyclohexanone yield using fresh and spent catalyst at $T = 190$ °C and 210 °C

No.	Time (min)	Fresh catalyst				Spent catalyst (after 60 h of usage) ^a			
		%Conversion		%Yield		%Conversion		%Yield	
		$T = 190$ °C	$T = 210$ °C	$T = 190$ °C	$T = 210$ °C	$T = 190$ °C	$T = 210$ °C	$T = 190$ °C	$T = 210$ °C
1	30	6.898	7.276	6.489	6.768	6.672	7.684	6.23	6.927
2	60	9.906	10.047	8.921	8.991	9.83	10.004	8.79	8.721
3	90	11.796	12.362	9.846	9.99	11.807	12.028	9.768	9.85
4	120	12.846	13.785	11.255	11.416	12.791	13.429	11.307	11.15
5	150	14.095	14.991	12.214	12.576	14.08	14.674	12.172	12.249
6	180	15.151	16.208	12.968	13.246	15.118	16.22	12.818	13.28
8	210	15.336	17.141	13.127	13.947	15.419	17.109	13.002	13.915
9	240	15.628	17.886	13.238	14.283	15.682	17.74	13.158	14.09

^a The 60 h of usage indicate the 15th run with the catalyst.

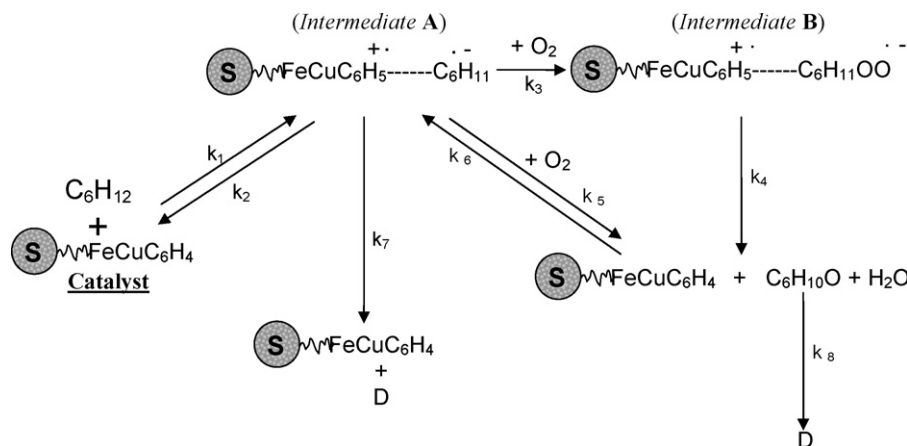


Fig. 11. A plausible ligand centered reaction mechanism for the oxidation of cyclohexane in presence of FeCu macrocyclic complex catalyst. Consistent with the experimental finding the cyclohexyl hydroperoxide is in the adsorbed state.

the kinetics and mechanism of cyclohexane oxidation in presence of MnAPO-5 catalyst. They have proposed that cyclohexyl hydroperoxide is an intermediate in cyclohexanol and cyclohexanone formation. Their combined rates of formation were found to be first order in ROOH concentration and proportional to the redox active Mn sites. Nunes et al. [48] have studied the mechanism and kinetics of cyclohexane oxidation (with iodobenzene) catalyzed by supramolecular manganese (III) porphyrins. They proposed a mechanism in which the cyclohexyl radical and OH groups combine rapidly to form cyclohexanol which is further oxidized to cyclohexanone. The free radical mechanism of cyclohexane oxidation occurs through the formation of cyclohexyl hydroperoxide intermediate in the reaction mass which decomposes to cyclohexanol and cyclohexanone (present in almost equimolar amounts). Since we have experimentally shown that the cyclohexyl hydroperoxide is not formed in the reaction mass we have proposed a reaction mechanism in which this intermediate is produced in the adsorbed state. For this, a ligand centered reaction mechanism has been proposed in Fig. 11. Since the concentrations of the product did not increase significantly as the reaction time was increased some of the reactions in Fig. 11 were taken to be reversible in nature. The cyclohexane molecule in presence of the catalyst first forms a cyclohexyl radical anion denoted as intermediate A (step 1). Intermediate A reacts with oxygen molecule forming a peroxy radical anion denoted as intermediate B (step 2) which

forms cyclohexanone as shown in step 3. The intermediate A also leads to the formation cyclohexanone when it reacts with oxygen as shown in step 4. Reactions shown in step 1 and step 4 are taken to be reversible in nature as the concentration of cyclohexane and cyclohexanone leveled off and does not show significant increase with increase in reaction time after 2 h. Consistent with the approach adopted in the literature, unidentified side products (D) are assumed to be formed from intermediate A (step 5) and cyclohexanone (step 6).

3.2.4. Determination of rate constants

Following this reaction mechanism, we can write a mole balance equations for each component of the reaction as given in Table 5. Using these, we have carried out simulation employing Runge–Kutta 4 method (as needed for the Genetic Algorithm in this specific code for optimal curve fitting) with $\Delta t = 0.01$ min for numerically stable solution and the concentration of each component was calculated. The results were optimized with the experimental values by using GA code and for this the objective function OF (given below) was written as the sum of squares of the difference of simulated and experimental values of cyclohexane and cyclohexanone.

$$OF = ([CH]_{sim} - [CH]_{exp})^2 + ([CHone]_{sim} - [CHone]_{exp})^2 \quad (1)$$

Table 5
Rate equation for each component

No.	Rate equation
1	$\frac{d[C_6H_{12}]}{dt} = -k_1[C_6H_{12}] + k_2[C_6H_{11}\bullet^-]$
2	$\frac{d[C_6H_{11}\bullet^-]}{dt} = k_1[C_6H_{12}] - k_2[C_6H_{11}\bullet^-] - k_3[C_6H_{11}\bullet^-][O_2] - k_5[C_6H_{11}\bullet^-][O_2] + k_6[C_6H_{10}O] - k_7[C_6H_{11}\bullet^-]$
3	$\frac{d[C_6H_{11}OO\bullet^-]}{dt} = k_3[C_6H_{11}\bullet^-][O_2] - k_4[C_6H_{11}OO\bullet^-]$
4	$\frac{d[C_6H_{10}O]}{dt} = k_4[C_6H_{11}OO\bullet^-] + k_5[C_6H_{11}\bullet^-][O_2] - k_6[C_6H_{10}O] - k_8[C_6H_{10}O]$
5	$\frac{d[O_2]}{dt} = -k_3[C_6H_{11}\bullet^-][O_2] - k_5[C_6H_{11}\bullet^-][O_2] + k_6[C_6H_{10}O]$
6	$\frac{d[D]}{dt} = k_7[C_6H_{11}\bullet^-] + k_8[C_6H_{10}O]$

Table 6
Rate constants at different temperature obtained by optimization using GA

Rate constants ($\text{m}^3/(\text{g catalyst})(\text{mol s})$)	$T=423\text{ K}$	$T=433\text{ K}$	$T=443\text{ K}$	$T=463\text{ K}$	$T=483\text{ K}$
k_1	6.8292E-03	8.9245E-03	1.2948E-02	1.7806E-02	2.0538E-02
k_2	1.7614E+00	2.3019E+00	2.9324E+00	3.3828E+00	3.5629E+00
k_3	8.6433E-01	1.0010E+00	1.2968E+00	1.6256E+00	1.6256E+00
k_4	4.8584E-01	1.3546E+00	1.6785E+00	2.1493E+00	2.1493E+00
k_5	1.4045E-02	8.9043E-02	4.2135E-01	6.0862E-01	7.9589E-01
k_6	1.4070E-05	3.2170E-05	5.0260E-05	8.6440E-05	8.6440E-05
k_7	2.4049E-03	4.3288E-03	5.2907E-03	7.2146E-03	9.1540E-03
k_8	7.2500E-05	9.0860E-05	1.0913E-04	1.4275E-04	4.1806E-04

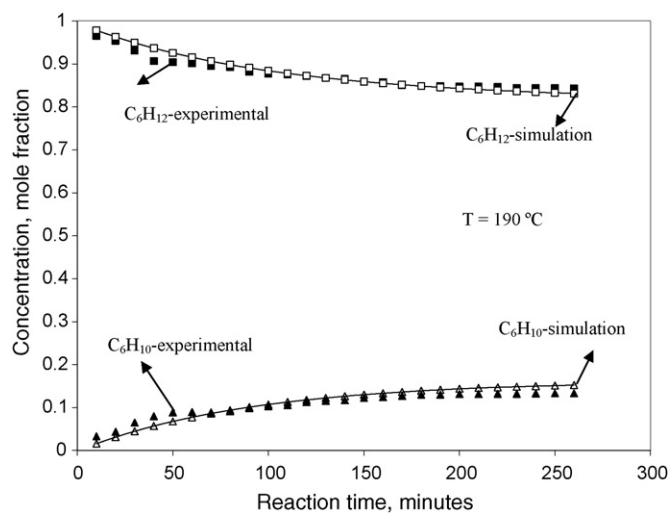


Fig. 12. Comparison of the simulated and the experimental results for $T=190\text{ }^\circ\text{C}$. The simulated results match the experimental data.

In the GA optimization, the fitness function is taken as $1/(1 + \text{OF})$ and its value of a single string is known as the string's fitness which is evaluated in each generation. The crossover and mutation probability were varied and finally taken at 0.9 and 0.05, respectively. The random population was created using a random number generator with a random seed equal to 0.887. The optimization was done for different temperatures and the results of fitting the data at $190\text{ }^\circ\text{C}$ are given in Fig. 12. The simulated concentrations overlap the experimental data and the best fit rate constants were determined which are reported in Table 6. The activation energy and the Arrhenius constant have also been calculated and are reported in Table 7. In Figs. 13 and 14 we have reported the concentrations of the intermediate species obtained

Table 7
Arrhenius dependence on rate constants

Rate constant	E/R	$\ln A$
k_1	3.80E+03	4.10E+00
k_2	2.31E+03	6.14E+00
k_3	2.28E+03	5.31E+00
k_4	4.29E+03	9.91E+00
k_5	7.95E+03	1.65E+01
k_6	5943.54	3.24
k_7	4162.220	4.02
k_8	6052.66	4.55

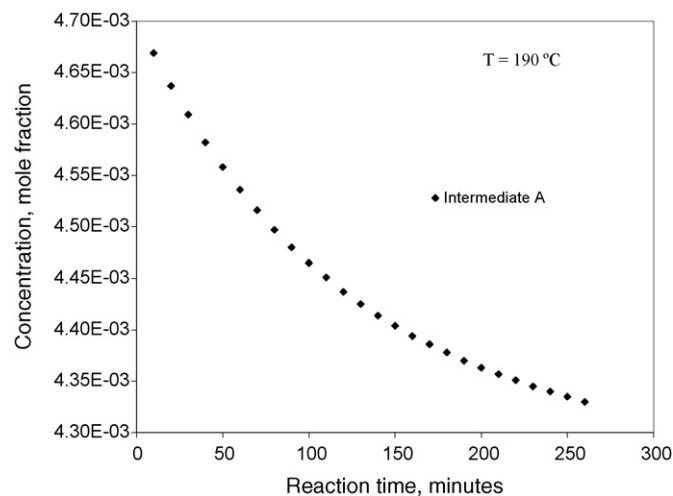


Fig. 13. The concentration of intermediate A obtained from simulation for $T=190\text{ }^\circ\text{C}$.

from simulation and it is observed that these concentration fall due to fall in amount of oxygen (Fig. 15) present in the reaction mass. This suggests that a higher oxygen pressure would favor the forward reaction giving high yield of the products. Unfortunately we could not run the reaction at higher pressures due to safety reasons.

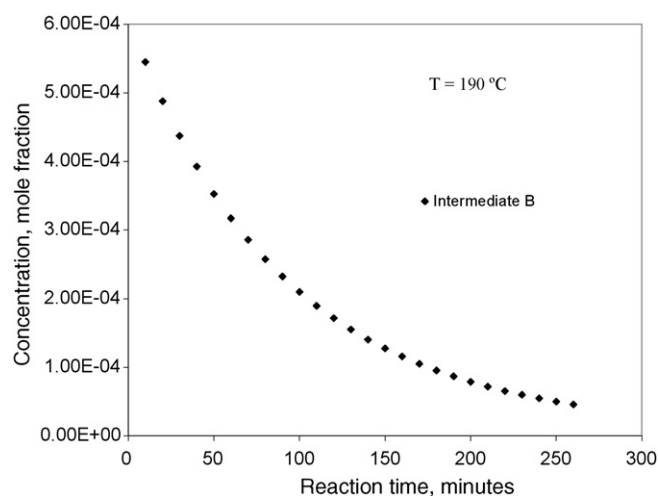


Fig. 14. The concentration of intermediate B obtained from simulation for $T=190\text{ }^\circ\text{C}$.

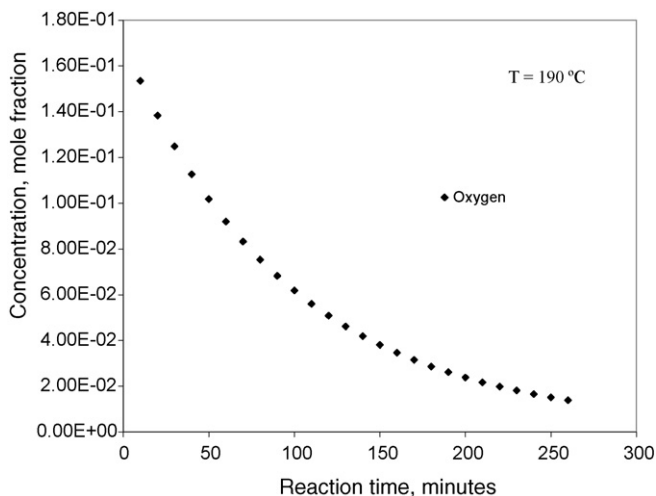


Fig. 15. The concentration of Oxygen obtained from simulation for $T = 190\text{ }^{\circ}\text{C}$.

4. Conclusion

In the present work, a heteronuclear bimetallic macrocyclic iron copper complex, $\text{FeCuL}(\text{NO}_3)_2 \cdot 4\text{H}_2\text{O}$ [$\text{L} = (\text{CH}_3\text{C}_6\text{H}_2\text{CH}_2\text{O}(\text{CH}_2)_3\text{N})_2$] has been prepared and this has been supported on zirconium pillared montmorillonite. The molecular structure of the complex was determined from X-ray diffraction analysis of the single crystal. The alternate occupancy of Fe and Cu atom was confirmed through this analysis. The CHN analysis of the complex was in close agreement with the theoretical value that was calculated from the structure of the complex. It was seen from the TGA that the final catalyst was stable up to $400\text{ }^{\circ}\text{C}$ while the complex was stable only up to $250\text{ }^{\circ}\text{C}$. From the small angle X-ray diffraction pattern it appears that there is a lack of ordering in the *c*-direction of the final catalyst. The oxidation of cyclohexane in the presence of this catalyst with molecular oxygen as the oxidant led to the formation of cyclohexanone along with uncharacterizable side products. At $190\text{ }^{\circ}\text{C}$ the cyclohexane conversion was 14.2% and cyclohexanone was formed with 87.4% selectivity. A ligand centered reaction mechanism, has been proposed based on the products formed. The optimal rate constants were determined using GA and the concentrations obtained from simulation were matched with the experimental data.

Acknowledgements

The authors thank the Department of Chemistry, IIT Kanpur, for the analytical measurements. We would also like to thank Prof. P.K. Bharadwaj and Ms. Vibha Mishra of Department of Chemistry, IIT Kanpur for helpful discussions and suggestion regarding single crystal X-ray studies.

References

[1] I.V. Berezin, E.T. Denisov, N.M. Emanuel, in: K.A. Allen (Ed.), *The Oxidation of Cyclohexane*, Pergamon Press, Oxford, 1966.
 [2] N.M. Emanuel, E.T. Denisov, Z.K. Maizus, *Liquid Phase Oxidation of Hydrocarbons*, Plenum press, New York, 1967.

[3] A.K. Suresh, M.M. Sharma, T. Sridhar, *Ind. Eng. Chem. Res.* 39 (2000) 3958–3997.
 [4] U. Schuchardt, D. Cardoso, R. Sercheli, R. Pereira, R.S. da Cruz, M.C. Guerreiro, D. Mandelli, E.V. Spinacé, E.L. Pires, *Appl. Catal. A: Gen.* 211 (2001) 1–17.
 [5] W.A. Carvalho, P.B. Varaldo, M. Wallau, U. Schuchardt, *Zeolites* 18 (1997) 408–416.
 [6] W.C.E. Arends, R.A. Sheldon, M. Wallau, U. Schuchardt, *Angew. Chem. Int. Ed. Engl.* 36 (1997) 1144–1163.
 [7] S.S. Lin, H.S. Weng, *Appl. Catal. A: Gen.* 118 (1994) 21–31.
 [8] A. Sakthivel, P. Selvam, *Mesoporous, J. Catal.* 211 (2002) 134–143.
 [9] J.W.M. Steeman, S. Kaarsemaker, P.J. Hoftyzer, *Chem. Eng. Sci.* 14 (1961) 139–149.
 [10] A.K. Suresh, T. Sridhar, O.E. Potter, *AIChE J.* 38 (1988) 69–80.
 [11] Y. Wen, O.E. Potter, T. Sridhar, *Chem. Eng. Sci.* 52 (1997) 4593–4605.
 [12] C.A. Tolman, J.D. Druliner, P.J. Krusic, M.J. Nappa, W.C. Siedel, I.D. Williams, S.D. Ittel, *J. Mol. Catal.* 48 (1988) 129–148.
 [13] C.A. Tolman, J.D. Druliner, M.J. Nappa, N. Herron, in: C.L. Hill (Ed.), *Alkane Oxidation studies in DuPont's Central Research Department, Ch. X in Activation and Functionalization of Alkanes*, John Wiley & Sons Inc., New York, 1989.
 [14] M. Spielman, *AIChE J.* 10 (1964) 496–501.
 [15] J. Alagy, P. Trombouze, H. Van Landeghem, *Ind. Eng. Chem. Proc. Des. Dev.* 13 (1974) 317–323.
 [16] R. Pohorecki, J. Baldgja, W. Moniuk, W. Podgorska, A. Zdrojowski, P.T. Wierchowski, *Chem. Eng. Sci.* 56 (2001) 1285–1291.
 [17] R. Pohorecki, J. Baldgja, W. Moniuk, A. Krysztoforski, Z. Wojcik, *Chem. Eng. Sci.* 47 (1992) 2559–2564.
 [18] V. Ponec, *Appl. Catal. A: Gen.* 222 (2001) 31–45.
 [19] W. Radecka-Paryzek, *Inorg. Chim. Acta* 35 (1979) 349–350.
 [20] W. Radecka-Paryzek, V. Patroniak-Krzyminiowska, *Collect. Czech. Chem. Commun.* 63 (1998) 363–370.
 [21] W. Radecka-Paryzek, *Inorg. Chim. Acta* 45 (1980) 147–148.
 [22] T. Tsubomura, K. Yasaku, T. Sato, M. Morita, *Inorg. Chem.* 31 (1992) 447–450.
 [23] L.K. Thompson, S.K. Mandal, S.T. Tandon, J.N. Bridson, M.K. Park, *Inorg. Chem.* 35 (1996) 3117–3125.
 [24] E. Spodine, Y. Moreno, M.T. Garland, O. Pena, R. Baggio, *Inorg. Chim. Acta* 309 (2000) 57–64.
 [25] N. Kuhnert, G.M. Rossignolo, A. Lopez-Periago, *Org. Biomol. Chem.* 1 (2003) 1157–1170.
 [26] S.J. Na, D.J. Joe, S. Sujith, W.-S. Han, S.O. Kang, B.Y. Lee, *J. Organomet. Chem.* 691 (2006) 611–620.
 [27] M. Thirumavalavan, P. Akilan, M. Kandaswamy, *Polyhedron* 24 (2005) 1781–1791.
 [28] P. Guerriero, S. Tamburini, P.A. Vigato, *Coord. Chem. Rev.* 139 (1995) 17–243.
 [29] B. Bosnich, *Inorg. Chem.* 38 (1999) 2554–2562.
 [30] C. Fraser, L. Johnston, A.L. Rheingold, B.S. Haggerty, C.K. Williams, J. Whelan, B. Bosnich, *Inorg. Chem.* 31 (1992) 1835–1844.
 [31] V.B. Romakh, B. Therrien, G. 'l Labat, H.S. -Evans, G.B. Shul'pin, G.-S. Fink, *Inorg. Chim. Acta* 359 (2006) 3297–3305.
 [32] V.B. Romakh, B. Therrien, L. Karmazin-Brelot, G. 'l Labat, H.-S. Evans, G.B. Shul'pin, G.-S. Fink, *Inorg. Chim. Acta* 359 (2006) 1619–1626.
 [33] G.B. Shul'pin, A.R. Kudinov, L.S. Shul'pina, E.A. Petrovskaya, *J. Organomet. Chem.* 691 (2006) 837–845.
 [34] K.S. Anisia, A. Kumar, *Appl. Catal. A: Gen.* 273 (2004) 193–200.
 [35] K.S. Anisia, A. Kumar, *J. Mol. Catal. A: Chem.* 219 (2004) 319–326.
 [36] K.S. Anisia, G.S. Mishra, A. Kumar, *J. Mol. Catal. A: Chem.* 215 (2004) 121–128.
 [37] G.S. Mishra, A. Kumar, *J. Mol. Catal. A: Chem.* 192 (2003) 275–280.
 [38] A. Kumar, G.S. Mishra, A. Kumar, *J. Mol. Catal. A: Chem.* 201 (2003) 179–188.
 [39] R.R. Gange, C.L. Spiro, T.J. Smith, C.A. Hamann, W.R. Thies, A.K. Shiemke, *J. Am. Chem. Soc.* 103 (1981) 4073–4081.
 [40] G.B. Shul'pin, *J. Mol. Catal. A: Chem.* 189 (2002) 39–66.

- [41] G.B. Shul'pin, C. R. Chim. 6 (2003) 163–173.
- [42] L.J. Farrugia, WinGX ver 1.64: An Integrated Systems of Windows Programs for the Solution, Refinement and Analysis of Single-crystal X-ray Diffraction Data, Department of Chemistry, University Of Glasgow, UK, 2003.
- [43] E.M. Serwicka, K. Baharnwoski, Catal. Today 90 (2004) 85–92.
- [44] F. Bedioui, Coord. Chem. Rev. 144 (1995) 39–68.
- [45] L.D. Gelb, K.E. Gubbins, R. Radha Krishnan, M. Silwinska Baratkowiak, Rep. Prog. Phys. 62 (1999) 1573.
- [46] L. Chmielarz, P. Kustrowski, M. Zbroja, A. Rafalska-Lasocha, B. Dudek, R. Dziembaj, Appl. Catal. B: Environ. 45 (2003) 103–116.
- [47] B. Modén, B. Zhan, J. Dakka, J.G. Santiesteban, E. Iglesia, J. Catal. 239 (2006) 390–401.
- [48] G.S. Nunes, I. Mayer, H.E. Toma, K. Araki, J. Catal. 236 (2005) 55–61.